PFG 2012 / 1, 0039–0050
Stuttgart, January 2012

Short Paper

System Theoretical Aspects for Designing Opto-Electronic Sensors for Remote Sensing

Ulrike Krutz, Anko Börner, Herbert Jahn, Carsten Paproth, Patrick Scherbaum & Emanuel Schlüssler, Berlin

Keywords: System theory, modelling, simulation, sensor systems

Summary: The design of passive optical sensor systems for remote sensing requires more or less complex theoretical investigations. Based on the user requirements which are characterized by data products all relevant physical effects influencing the generation of an image have to be considered and modeled. The goal is to build the whole chain of signal generation and transformation: from the source of light, through the atmosphere to the object to be observed, through the atmosphere back to the sensor system. These models can be applied to simulations which can be used for the optimization of sensor parameters and observation conditions and for the estimation of the potential performance of such a system. For this task, specific retrieval algorithms have to be considered closing the loop of developing camera systems.

The paper contains classical approaches for a system design as a standard tool used in the Institute for Robotics and Mechatronics including methods for modeling the geometrical and radiometric relations and the description of camera hardware. The results of a complex investigation of the point spread function of camera systems form the core topic of this paper.

Zusammenfassung: *Systemtheoretische Aspekte zum Design von opto-elektronischen Sensoren für die Fernerkundung.* Die Auslegung von passiven optischen Sensorsystemen für die Fernerkundung erfordert je nach Applikation mehr oder minder komplexe Voruntersuchungen. Ausgehend von den Nutzeranforderungen an ein Kamerasystem, die in der Regel durch Datenprodukte charakterisiert werden, müssen alle relevanten physikalischen Effekte, die zur Generierung eines Bildes beitragen, berücksichtigt und modelliert werden. Ziel ist es, die gesamte Kette der Signalentstehung und -wandlung nachzubilden: vom Beobachtungsobjekt und seiner Beleuchtungsquelle, über die Atmosphäre bis hin zum Sensorsystem. Diese Modelle können in Simulationsrechnungen einfließen, die die Optimierung von Sensorparametern und Aufnahmebedingungen sowie die Bewertung des Potenzials eines solchen Systems gestatten. Für diese Aufgaben müssen konkrete Auswertealgorithmen in den Entwurfsprozess einfließen, womit sich der Entwicklungskreis schließt.

Der Beitrag umfasst klassische Ansätze zur Systemauslegung, die im Institut für Robotik und Mechatronik verfolgt werden. Darunter fallen Verfahren zur Modellierung der geometrischen und radiometrischen Verhältnisse sowie die Beschreibung der Hardware der Kamera. Die Ergebnisse einer beugungstheoretischen Untersuchung zur Punktverschmierungsfunktion von Kamerasystemen bilden den Schwerpunkt dieser Arbeit.

1 Introduction

In the 1980s the opto-electronic sensor department of the Institut für Kosmosforschung in Berlin-Adlershof started to design passive imaging sensors for remote sensing. One of the first projects in that direction was the design of a spaceborne imaging sensor for the detection of ocean waves and the estimation of wave parameters (Jahn et al. 1989). In that connection the idea arose to model and simulate the whole system comprising of the light source (blue sky light), the atmosphere, the scene (ocean water with waves), and the optical and

www.schweizerbart.de
DOI: 10.1127/1432-8364/2012/0101
1432-8364/12/0101 $ 3.00

electronic parts of the sensor up to the image data in order to obtain optimal system performance for wave parameter determination. At the same time CCD sensors became available and have been studied carefully (Oertel et al. 1985). After those first approaches the system theoretic aspects of opto-electronic sensor systems were developed in more detail resulting in a book (Jahn & Reulke 1995), in simulation software packets (Jahn et al. 1992, Börner et al. 2001), and in the design of various sensors, e. g. WAOSS (Sandau & Eckardt 1996, Sandau et al. 2000), HSRS for the small satellite BIRD (Bi-Spectral Infrared Detection) (Skrbek & Lorenz 1998) and others. This work is now carried on in DLR's department of Optical Information Systems in various projects e. g. MERTIS (Arnold et al. 2009). In more detail, the system theoretic approach to remote sensing systems comprises the description and modelling of:

- the emitted radiances of the light source, e. g. a light reflecting and/or emitting surface with its physical and geometrical parameters,
- the atmospheric path of the radiation (radiation transfer, use of software packages, e. g. MODTRAN),
- the optical system with its fundamental parameters such as point spread function (PSF), modulation transfer function (MTF) and others,
- the opto-electronic detector with its characteristics (quantum efficiency, PSF, photo-response non-uniformity (PRNU), dark signal non-uniformity (DSNU) etc.),
- the electronic read-out channel with its impulse response,
- the analogue digital unit (ADU),
- the various noise components of all these components and, last but not least,
- the data evaluation algorithms, e. g. for object detection or classification.

The goal of that approach is to fulfil the scientific objectives of the project as optimally as possible, under certain constraints such as available technology and money. Ideally, the evaluation algorithm provides a quality criterion, e. g. for parameter estimation or classification, which depends on system parameters such as focal length, integration time etc. Then, minimizing that criterion provides optimal system performance. Of course, that approach often cannot be carried out in full purity but it gives a good guideline for system design. Additionally, observation conditions, e. g. orbit, season, time, and retrieval algorithms can provide input for an overall optimizing approach.

2 Modelling Approaches

The following paragraph describes typical approaches for system modeling. Depending on the project phase (from pre-studies to final system design) more or less complex models are applied.

2.1 *Derivation of Top Level Requirements*

Based on user requirements (geometrical resolution, swath width, number and position of spectral bands), technical top level requirements of the camera system are derived. For the design of imaging optical systems signal-to-noise ratio (SNR), MTF (typically at Nyquist frequency), wavelength and bandwidth of spectral bands and radiometric dynamics are the most important quantities defining parameters such as focal length, size of aperture, system clock and data rate. These optical and electronic system parameters are used to perform a first estimation about the expected system performance. As a basic input qualitative and quantitative information about incident light being reflected or emitted from the object to be observed is required. For this purpose, realistic at-sensor radiances have to be estimated by applying atmospheric transfer models, e. g. MODTRAN. The number of photons is converted into electrons considering optics and detector parameters. Most dominant noise sources are estimated to calculate the system's SNR.

The geometric resolution of a camera system is defined by ground sample distance, blur due to optical diffraction, motion of the camera during capturing the image and SNR. Usually, Rayleigh criterion is applied defining the distance of two single spots which can

be distinguished considering the effects mentioned above.

Such rough calculations are basic input for proposals for remote sensing missions for Earth observation or planetary research.

For concrete system designing and optimizing system parameters, more complex approaches have to be pursued. The next chapters describe tools supporting theses tasks. In general, geometrical and radiometric relations have to be considered as well as the hardware parameter of the opto-electronic system.

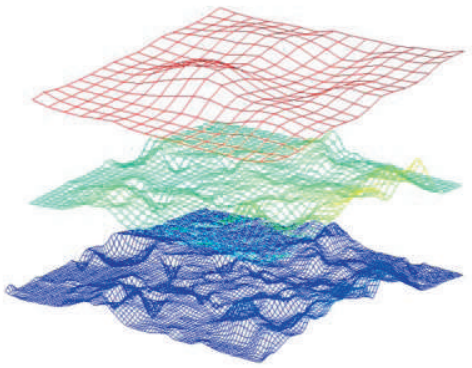

Fig. 1: The DTM is used in different resolutions to decrease aliasing.

2.2 *Geometric Properties*

The challenge of the geometry module of the sensor simulation is to figure out to which direction each camera pixel is geared. For this purpose, a simple ray tracing approach is taken. Therefore, a digital terrain model (DTM) and a camera model as input are essential. Then the intersections of each ray can be investigated, constructed from the camera description for each pixel, with the DTM. The nearest intersection is taken as result. Furthermore, the same procedure can be applied to determine whether the area is shadowed or not, simply by using rays from the intersection points to the sun. If there is a nearer intersection between the DTM and the sun, then the observed area is shadowed. Finally, we obtain the following information from the geometry module for each camera pixel:

- the intersection point in Cartesian and geodetic coordinates,
- the surface normal at the intersection point,
- the Boolean shadow value,
- accompanying map values, e. g. albedo and temperature.

These results are needed for the radiometry module of the sensor simulation.

The described rendering procedure and with it the resulting camera images can suffer from the sample problem which results in aliasing due to under-sampling of the scene. To decrease the effect of aliasing, we can increase the resolution of the camera model, i. e. use more rays per pixel, or reduce the resolution of the geometric description of the scene, i. e. use a lower resolution DTM. The increasing of rays per pixel improves the image quality, but it also increases the computing power needed for one camera image. Lower space-resolved DTMs are part of this multi-resolution ray tracing approach. Starting point is a spatially high-resolution DTM from which the lower resolution models are created. This model is transformed into a pyramid of models where each model obtains only half of the linear resolution of the previous model, see Fig. 1. During the ray tracing procedure, the model with the best fitting resolution is chosen according to the ground resolution seen from the camera.

Moreover, the geometry module makes it possible to cover the interesting area with tiles. The size of the individual tiles can be kept small so that the need for memory is low for one tile. During the ray tracing only the currently needed tiles are kept in memory. The available memory is managed with a caching strategy. By this innovation, the area can be covered by terrain models with different resolutions, e. g. Germany as a whole can be covered by a DTM with low resolution while specific areas are considered with a high-resolution DTM.

2.3 *Radiation Transfer Models*

For the simulation of a sensor, the radiometric behaviour has to be specified (Börner et al. 2001). This is done with the radiometry module which calculates the at-sensor radiance

for every pixel of the camera from the visible spectral range to the thermal infrared. This module uses MODTRAN (Berk et al. 1987) for the radiative transfer through the atmosphere. The module works in two steps. The first step is the creation of a spectral look-up table for the global atmosphere parameters. In the second step this look-up table is applied to create spectral radiances for the local simulation parameters, e. g. albedo and surface normal. This procedure is much faster than the direct usage of MODTRAN and produces similar results. The required input parameters of MODTRAN are: spectral range and step size; average ground height; sensor altitude; sensor zenith angle; atmospheric model; haze model; visibility; sun zenith angle; albedo ρ and temperature T. Unless specified, the MODTRAN default values are used.

The at-sensor radiance can be written as a sum of five addends, see Fig. 2,

$$L(\lambda) = L_{dir} + L_{ind} + L_{sc} + L_{em} + L_{th} \tag{1}$$

The indirect and scattered contributions L_{ind}, L_{sc} and L_{th} are calculated directly with MODTRAN and are part of the lookup table. The direct and emitted contributions can be calculated with

$$L_{dir} = L_{sun} \cdot \cos\alpha \cdot \rho \cdot s \tag{2}$$

and

$$L_{em} = B(T) \cdot (1-\rho) \cdot \tau \tag{3}$$

with the solar irradiance L_{sun} and the transmittance of the atmosphere τ, which are also part of the lookup table. The angle between the surface normal and the incident light α as well as the Boolean shadow variable s are both results of the geometry module. With the spectral radiance of a blackbody $B(T)$ mapped values of ρ and T can be used to complete the radiometric simulation of a whole camera image without using MODTRAN directly for every camera pixel. Finally, the spectral at-sensor radiance for the corresponding spectral range gets convolved with a rectangular function to achieve the desired spectral step size and to avoid aliasing. The resulting spectrum is passed onto the camera module, which accomplishes the final processing. An example spectrum is shown in Fig. 3.

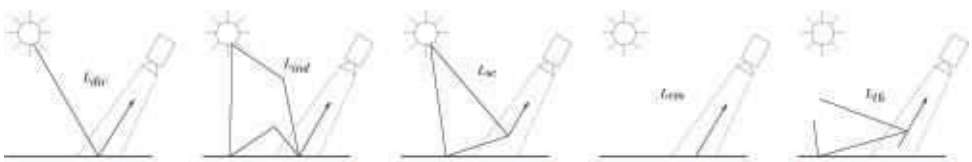

Fig. 2: MODTRAN calculates these contributions to the at-sensor-radiance: L_{dir} is the direct reflected solar radiance, L_{ind} is the indirect reflected solar radiance, L_{sc} is the scattered solar radiance, L_{em} is the emitted thermal radiance, and L_{th} is the scattered thermal radiance.

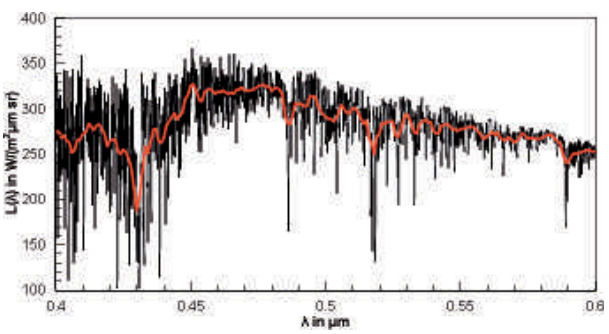

Fig. 3: Spectral at-sensor radiance for a mid-latitude summer atmosphere, sun at the zenith, sensor altitude 100 km, and ρ = 0.5. The red curve is the convolution of the at-sensor radiance with an appropriate rectangular function for a spectral step size of 1 nm.

2.4 *Camera Models*

By modelling the camera, the geometrical and physical properties of optics and sensor are simulated. The first step is the provision of data for further processing for the Raytracer. Then, the results of the radiometric simulation can be processed. The Raytracer requires the normalized direction vector for each pixel. The camera includes the position of each pixel in relation to the projection centre. With this position and the position of the principal point, the Raytracer can generate the direction vector (Fig. 4). With these pixel positions the geometric characteristics of various detector types such as Matrix, Line, Staggered and TDI can be modelled.

The output data of the radiometric simulation is represented by the at-sensor radiance. Out of this data, the digital number (DN) has to be calculated by the camera module. Therefore, the number of electrons which are liberated by the photons must be determined:

$$n_{el} = \frac{\pi}{4} \cdot \frac{1}{f_{\#}^2} \cdot A_d \cdot f_f \cdot t_{\text{int}} \int_{\lambda_1}^{\lambda_2} d\lambda \frac{\lambda}{h \cdot c} \cdot L(\lambda) \cdot \tau(\lambda) \cdot QE(\lambda) \tag{4}$$

where $f_{\#}$ is the f-number of the optical system, A_d the area of a pixel, f_f the fill factor of a sensor element, t_{int} the integration time, λ the wavelength, $L(\lambda)$ the radiance (eq. 1), τ the transmission of the optical system and QE the quantum efficiency. Furthermore, h denotes the Planck constant and c the speed of light in vacuum.

If the bit depth (Depth) and the full well capacity ($\text{Cap}_{\text{FullWell}}$) of the detector are known entities, the digital number can be calculated by quantization, as shown in the following formula:

$$DN = \frac{n_{el} \cdot \left(2^{Depth} - 1\right)}{Cap_{FullWell}} \tag{5}$$

The full well capacity determines the maximum number of electrons which the detector can generate. Furthermore, it represents a gain level which is used for the exposure. These simulated results usually do not correspond to reality. However, when the distortion model of the optics and the noise model of the sensor are known, it is possible to derive a result that reflects reality (Hartley & Zissermann 2003).

3 Investigation of PSF

The previous section dealt with a geometrical and a radiometric approach of camera description. Now, a diffraction-theoretical approach follows, taken into account the point spread function (PSF). Consider a system like in Fig. 5. Here, g denotes the distance between object plane and the optics and f the focal length. Furthermore, n and n'' represent normal vectors, U' the amplitude right behind the object plane and V the amplitude right in front of the optics. Likewise, V' describes the amplitude immediately behind the optics and U the amplitude in front of the image plane.

By mapping a point P' of the object plane to the image plane, the point is blurred by the PSF. For translation-invariant systems the following equation is valid

$$b(P'') = \int_{-\infty}^{\infty} dP' \, \hat{g}(P') \cdot H(P'' - P') = (\hat{g} * H)(P'') \tag{6}$$

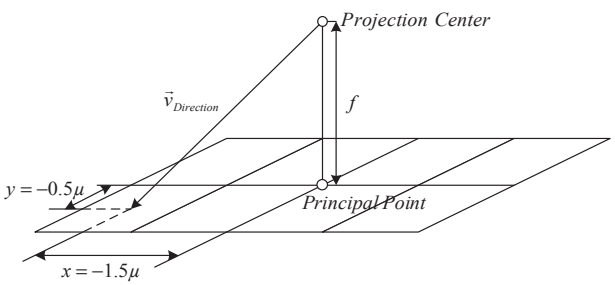

Fig. 4: Direction vector of a pixel as used in a Raytracer.

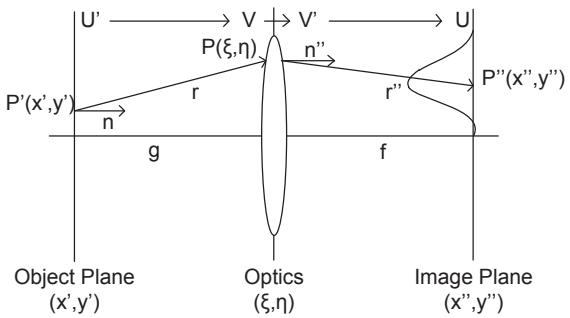

Fig. 5: Mapping a point *P'* of the object plane (x', y') to the image plane (x", y") underlies impairments caused by the system's point spread function. g is the object distance, *P*' the emitting point, *P*'' the image of the emitting point *P*', *f* is the focal length, which is in the general case the image distance (b). ξ and η are the coordinates in the lens frame. ξ" and η" are the coordinates in the image frame. r and r" are the corresponding direction vectors.

where b is the image, H the PSF and $\hat{g}$ the point's intensity on the image plane.

The resulting image underlies all impairments caused by the system's total PSF. Let the system now be separable, so that it can be split into the components optics and detector. Furthermore, motion and eventually the atmosphere contribute to a blurring of the original signal. This blurring finds its expression in the successive convolution of the signal with the according point spread function of the system components.

3.1 *PSF of the Optics*

There are at least three different ways to determine the PSF of optics in theory, among quite a few possibilities to determine it in a practical way (Talbiersky 2010, Jahn & Reulke 1995). In theory the PSF of optics can be either calculated by the Kirchhoff diffraction formula, the Fresnel- or the Fraunhofer formula. Here, Kirchhoff is the origin for both, Fresnel, which is a square approximation, and Fraunhofer, which approximates Kirchhoff in a linear way. Like in Cooper et al. (2002) the Kirchhoff formula used here underlies the Kirchhoff boundary conditions (Born & Wolf 1999) as it is assumed that at the edge of the aperture the amplitude of the wave of the object to be imaged turns to zero quite suddenly. In practice this is mostly not the case. Furthermore, the polarization of light is ignored and the calculations are based on scalars rather than on vectors. Therefore, the Kirchhoff diffraction formula itself is only an approximation of the exact issue.

The PSF by Kirchhoff is given by the following formula (Jahn & Reulke 1995)

$$H_{\lambda}^{OPT}(P',P'') = \left| e^{\frac{2\pi i}{\lambda}\cdot n_{\lambda}\cdot\Delta} \iint_{O_L} d\xi d\eta \, e^{-\frac{\pi i}{\lambda f}(\xi^2+\eta^2)} \cdot \frac{e^{\frac{2\pi i}{\lambda}|\underline{r}''|}}{i\lambda|\underline{r}''|} \cdot \frac{\underline{n}''\cdot\underline{r}''}{|\underline{n}''|\cdot|\underline{r}''|} \cdot \frac{e^{\frac{2\pi i}{\lambda}|\underline{r}|}}{i\lambda|\underline{r}|} \cdot \frac{\underline{n}\cdot\underline{r}}{|\underline{n}|\cdot|\underline{r}|} \right|^2 \quad (7)$$

where $r = \begin{pmatrix} \xi - x' \\ \eta - y' \\ g \end{pmatrix}$ and $r'' = \begin{pmatrix} \xi'' - x' \\ \eta'' - y' \\ b \end{pmatrix}$. Furthermore, λ is the wavelength, n_{λ} the refractive index and Δ the maximal diameter of the lens. The other parameters are the same as in Fig. 5. Obviously, this formula appears to be quite cumbersome. Fresnel approximations offer a large variety of advantages such as the way of simplifying modeling diffraction effects due to the replacement of a square root in a phase term by a quadratic form and minor other changes. Moreover, there are quick ways of implementing Fresnel (Mendlovic et al. 1997). This is especially the case for diffraction-limited systems as the PSF by Fresnel can be solved analytically by using polar coordinates. The result is the Bessel function J_1:

$$H_{\lambda}^{OPT}(P',P'') = \left| G \cdot 2 \cdot \pi \cdot R^2 \cdot \frac{J_1\left(\frac{2\pi}{\lambda b} \cdot \rho \cdot R\right)}{\frac{2\pi}{\lambda b} \cdot \rho \cdot R} \right|^2 \quad (8)$$

Where R is the radius of the lens, λ the wavelength, ρ the distance in the image frame (or x''-y''-frame) from the centre point of the PSF, and $G := -\frac{e^{\frac{2\pi i}{\lambda}(b+g)}}{\lambda^2 \cdot b \cdot g} \cdot e^{\frac{\pi i}{\lambda b}(x''^2+y''^2)} \cdot e^{\frac{\pi i}{\lambda g}(x'^2+y'^2)} \cdot e^{\frac{2\pi i}{\lambda} n_\lambda \Delta_0}$.

The diffraction pattern is the well-known Airy disk.

Let $P' = (x',y') = (0,0)$ and $P'' = (x'',y'') = (0,0)$ be on-axis observation points. In the following (P',P'') is represented by the vector $\underline{0}$. By using polar coordinates eq. 7 is transferred into

$$H_{\lambda}^{OPT}(\underline{0}) = \left| -\int_0^R dr \; \frac{2\pi bg}{\lambda^2} \cdot \frac{e^{-\frac{\pi i}{\lambda f} r^2} \cdot e^{\frac{2\pi i}{\lambda}\left(\sqrt{r^2+b^2}+\sqrt{r^2+g^2}\right)}}{\left(r^2+b^2\right)\cdot\left(r^2+g^2\right)} \cdot r \right|^2 \quad (9)$$

Likewise the PSF for Fresnel is

$$H_{\lambda}^{OPT}(\underline{0}) = \left| -\int_0^R dr \; \frac{2\pi}{\lambda^2 bg} \cdot e^{\frac{2\pi i}{\lambda}(b+g)} \cdot r \right|^2 \quad (10)$$

Unfortunately, the advantages of Fresnel cannot be used for arbitrary camera systems. For configurations with wide aperture, e. g., the application of Fresnel approximation is not possible without accepting an unagreeable deviation. In Figs. 6 and 7 this effect is shown for a laboratory configuration with a focal length $f = 0.02\ m$, ground distance $g = 1\ m$ and a varying f-number. For low f-numbers the percentage mistake – regarding to the maximal values of the PSF of Kirchhoff and Fresnel – nearly hits 100 % while the mistake tends to zero for f-numbers greater than 6.

Consider now the real and complex integrands of eq. 9 and eq. 10.

As can be seen in Fig. 8 and Fig. 9, the formula of Fresnel approximates the formula of Kirchhoff quite well for small apertures. For bigger values of r, Kirchhoff begins to oscillate – Fresnel cannot be used as an approximation anymore. The first zero of the complex integrand can be taken as a criterion up to which maximal aperture radius the formula

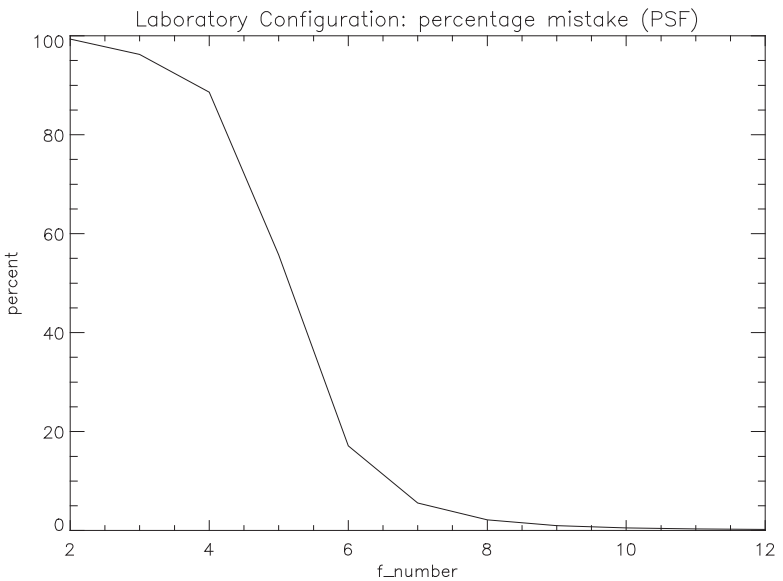

Fig. 6: Percentage mistake (PSF), regarding to the maximal values of the PSF of Kirchhoff and Fresnel.

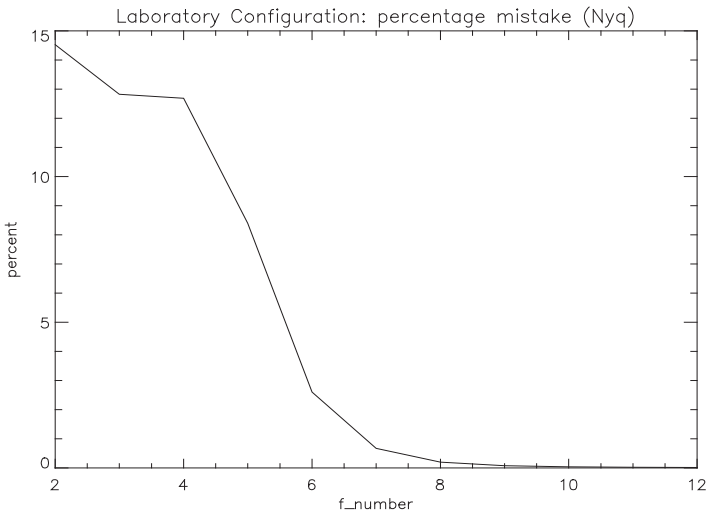

Fig. 7: Percentage mistake (at Nyquist frequency), regarding to the maximal values of the PSF of Kirchhoff and Fresnel.

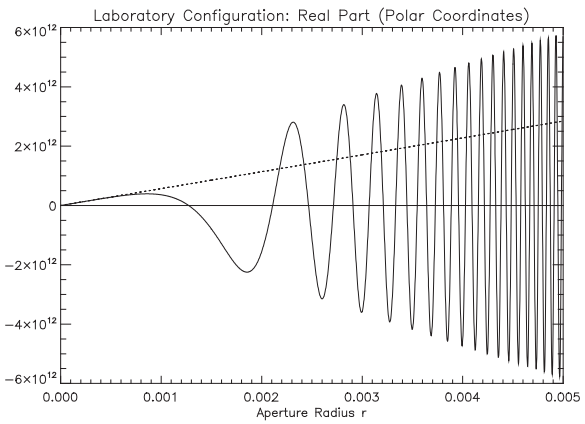

Fig. 8: Real Part of integrand.

by Fresnel can be used instead of Kirchhoff's. An analytical determination of zero leads to an equation from which the minimal f-number is derived, so that Fresnel approximations can still be applied to a system:

$$f_{\#\min} = \frac{\gamma}{2 \cdot R_{zero}} \tag{11}$$

with

$$R_{zero} = \sqrt[4]{\frac{8(\alpha+\beta)-2l}{\frac{1}{\alpha^3}+\frac{1}{\beta^3}}}, \alpha := \frac{g}{\lambda}, \beta := \frac{b}{\lambda}, \gamma := \frac{f}{\lambda}$$

and l the first zero of the imaginary part or the real part of the integrand, depending on even or odd l.

For the laboratory configuration the zeros are calculated to $r_1 = 0.0013$ and $r_2 = 0.0018$. The error interval therefore is [0.2 %, 5 %] and the F-numbers range between ~ 6 (resulting from r_2) and ~ 8 (resulting from r_1). If one compares these values with the former results for different f-numbers it is significant that the bigger one of the first two zeros provides the minimal f-number for which the usage of the Fresnel formula is possible.

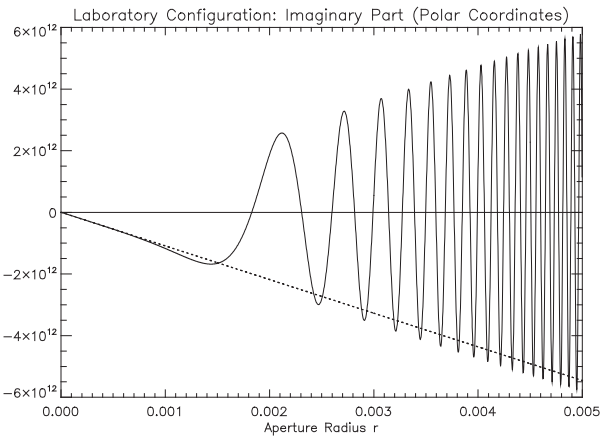

Fig. 9: Imaginary part of integrand.

Due to ignorance of the true PSF it is often convenient to use a simplified PSF-model represented by the following Gaussian function instead of the formulas given above:

$$H_{\lambda}^{OPT}(P',P'') = \frac{1}{2\cdot\sigma^2\cdot\pi}\cdot\left(\frac{f}{g}\right)^2\cdot e^{-\frac{1}{2\sigma^2\left[\left(\frac{f}{g}x'+x''\right)^2+\left(\frac{f}{g}y''+y''\right)^2\right]}} \quad (12)$$

where $\sigma_x = \sigma_y = \sigma$. If the object distance is not fixed, but varies with the time, the PSF results into

$$H_{\lambda}^{OPT}(P',P'',t) = \frac{1}{2\cdot\sigma^2\cdot\pi}\cdot\int_0^{t_{\text{int}}} dt\left(\frac{f}{g(t)}\right)^2\cdot e^{-\frac{1}{2\sigma^2\left[\left(\frac{f}{g(t)}x'+x''\right)^2+\left(\frac{f}{g(t)}y''+y''\right)^2\right]}} \quad (13)$$

3.2 *PSF of Motion*

The PSF of motion has to be considered whenever movement occurs between camera and object, nevertheless whether the camera or the object or both are the moving elements. In this section motion in x- and in y-direction are taken into account. The motion in z-direction effects the PSF of optics as can be seen in eq. 13 with g instead of z. Let $s(t) = s(0) + \int_0^{t_{\text{int}}} dt\, v(t)$ describe the distance that a mapped point with a certain velocity $\underline{v}(t) = (v_x(t), v_y(t), v_z(t))$ covers on the CCD during the integration time. To obtain the PSF of motion, a moving light impulse represented by the term $\delta(x-s_x(t))\cdot\delta(y-s_y(t))$ has to be integrated over a certain time span. This results into

$$H^M(x,y) = \frac{1}{t_{\text{int}}}\sum_k \frac{1}{\left|v_x(t_k)\right|}\cdot\delta\left(y-\int_0^{t_k} dt'\, v_y(t')\right)\cdot R_{t_{\text{int}}}\left(t_k-\frac{t_{\text{int}}}{2}\right) \quad (14)$$

where t_k denotes the zeroes of the equation

$$\varphi(t) := \int_0^t dt'\, v_x(t') - x = 0 \quad (15)$$

and $R_{t_{\text{int}}}(t)$ the rectangular function.

Let the motion be random $v_x(t) = \sin(\omega t)$, $v_y(t) = \cos(\omega t)$ and represent, e. g. the jitter of an airplane restricted by the angle $\alpha < \frac{\pi}{2}$. The integration time is $t_{\text{int}} = \frac{\alpha}{\omega}$. Furthermore let $x \in [0, t_{\text{int}}]$ where $t_{\text{int}} < \frac{\pi}{2\omega}$. Then the PSF of motion is given by

$$H^M(x,y) = \frac{1}{t_{\text{int}}}\cdot\frac{1}{\left|\frac{1}{\omega}\cos(\omega t_0)\right|}\cdot\delta\left(\cos(\omega t_0)-y\right)\cdot R_{\frac{\alpha}{\omega}}\left(t_0-\frac{\alpha}{2\omega}\right) \quad (16)$$

where $t_0 = \frac{1}{\omega}\sin^{-1} x$ is the only zero of eq. 16. In contrast to the PSF of the optics, a point source mapped onto the CCD is not blurred to a disk, but rather stretched to a line.

3.3 *PSF of the Detector*

Let the detector be ideal, i. e., a rectangle with the side lengths Δ_x and Δ_y. Furthermore the whole surface shall be of the same sensitivity. Then the PSF of the detector can be represented by

$$H^D(x,y) = \begin{cases} \frac{1}{\Delta_x \Delta_y} & for -\frac{\Delta_x}{2} \le x \le \frac{\Delta_x}{2}, -\frac{\Delta_y}{2} \le y \le \frac{\Delta_y}{2} \\ 0 & else \end{cases} \quad (17)$$

3.4 *Total PSF*

The total PSF of the system is obtained by the successive convolution of the PSFs of the system components and the PSF of motion. Before the original signal is smeared by the PSF of the optics, also the PSF of the atmosphere might contribute to the blurring. The PSF of the atmosphere can be approximated by a 2-dimensional Gaussian function like the one in eq. 12. A more detailed description can be found in Krishnakumar & Venkatakrishnan (1998). If this PSF has to be taken into account – whether yes or no depends on the project – both functions have to be convolved:

$$H^{(2)}(x,y) = \iint_{O_L} d\xi d\eta \; H^{OPT}(x-\xi, y-\eta) \cdot H^{ATM}(\xi,\eta) \quad (18)$$

If the atmosphere can be neglected, it is $H^{(2)}(x,y) = H^{OPT}(x,y)$. Then it is

$$H^{(3)}(x,y) = \iint_{O_L} d\xi d\eta \; H^{D}(x-\xi, y-\eta) \cdot H^{(2)}(\xi,\eta) \quad (19)$$

At last the PSF of motion smears the signal, so that the total PSF is obtained:

$$H^{total}(x,y) = \iint_{O_L} d\xi d\eta \; H^{M}(x-\xi, y-\eta) \cdot H^{(3)}(\xi,\eta) \quad (20)$$

A detailed description of the results can be found in (Krutz 2011).

4 Simulation and System Optimization

Based on the models of all relevant components of a complex system (including source of light, atmosphere, object, camera) computer simulations will be performed in order to recreate the real world and the behaviour of the opto-electronic system before it is built. The models are implemented into program languages (typically IDL, C, C++), all relevant input parameters of theses models can be set allowing the run of batches. These simulations

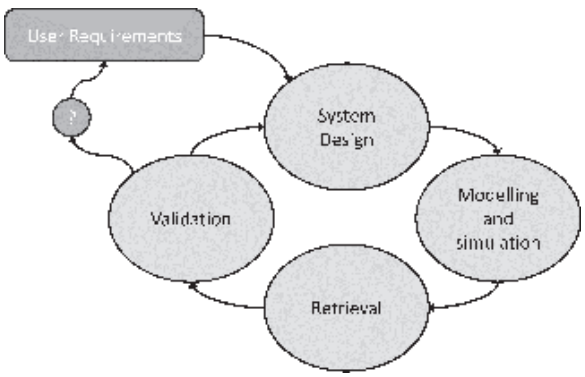

Fig. 10: Typical development cycle using models and simulation.

will result in virtual data which can be analyzed by dedicated retrieval algorithms deriving quantities which can be compared directly with user requirements. Modeling and Simulating allows the definition if a development cycle as depicted in Fig. 10.

Based on user requirements, technical top-level requirements will be derived. These parameters are used for a first system design being input for modeling and simulations. Outcoming virtual data can be processed with retrieval algorithms allowing a comparison between users expectations and systems capabilities. If necessary, system design, observation conditions and/or retrieval algorithms have to be adapted until an optimization criterion is reached.

As an example, the optimization cycle of a star sensor will be described. Starting with user requirements (pointing knowledge), top level parameters of the camera will be derived (focal length, SNR, MTF). These values will be used to define a camera model which enables the developing team to simulate images taken by this virtual camera under certain conditions (e. g. the camera's viewing direction). These images include all relevant effects, e. g. noise and blur. A retrieval algorithm then detects stars, performs an object matching with the star catalogue and determines viewing direction of the camera. The deviation between input viewing direction and determined viewing direction is an error criterion, which shall be minimized. This error minimization or system optimization is realized by dedicated changing of relevant parameters of the whole system, e. g. reducing the jitter of the satellite bus, improving optical MTF.

5 Conclusion and Outlook

Designing optical payloads for dedicated scientific or commercial tasks requires a precise analysis of the complete system including the environment and the sensor system itself based on physical models. Considering all relevant parameters of the object to be observed, the radiative transfer and the opto-electronic device allow the optimization of the all-over system chain with respect to performance and costs. Such an approach is worthwhile and indispensable for detector systems for remote sensing applications against the background of steadily increasing user requirements, limited ressources, operational availability and high accuracy and reliability.

Future work will be focussed on investigations on new optical technologies, e. g. potential of segmented and synthetic apertures, new detectors, e. g. sCMOS cameras, sensor data fusion, e. g. potential of radar / optics fusion / hyperspectral infrared systems, for applications in Earth observation and Planetary exploration.

References

Arnold, G., Hiesinger, H., Helbert, J., Paproth, C., Säuberlich, T., Peter, G. & Walter, I., 2009: Thermal Infrared Imaging of Mercury – MERTIS – a New Remote Sensing Technology. – Infrared Spaceborne Remote Sensing and Instrumentation XVII, Proceedings of the SPIE **7453**, San Diego, CA, USA.

Berk, A., Bernstein, L.S. & Robertson, D.C., 1987: MODTRAN: A Moderate Resolution Model for LOWTRAN. – Techical Report, Air Force Geophysics Laboratory.

Born, M. & Wolf, E., 1999: Principles of Optics. – **7th**, Cambridge University.

Börner, A., Wiest, L., Reulke, R., Richter, R., Keller, P., Schaepman, M. & Schläpfer, D., 2001: SENSOR: a Tool for the Simulation of Hyperspectral Remote Sensing Systems. – ISPRS Journal of Photogrammetry and Remote Sensing **55:** 299–312.

Cooper, I., Sheppard, C. & Sharma, M., 2002: Numerical Integration of Diffraction Integrals for a Circular Aperture. – Optik. – International Journal for Light and Electron Optics **113** (7): 293–298.

Hartley, R. & Zissermann, A., 2003: Multiple View Geometry in Computer Vision. – **2nd**, Cambridge University Press, Cambridge, UK.

Jahn, H. & Reulke, R., 1995: Systemtheoretische Grundlagen optoelektronischer Sensoren. – 253, Akademie Verlag, Berlin.

Jahn, H., Oertel, D., Sandau, R. & Zimmermann, G., 1989: Aspects of the Determination of Ocean Wave Parameters by Means of an Optoelectronic Satellite Sensor. – Acta Astronautica **19** (6–7): 513–519.

Jahn, H., Reulke, N. & Reulke, R., 1992: Simulation von Bilddaten für die Mars-Missionen. – Bild & Ton **45:** 276–281.

Krishnakumar, V. & Venkatakrishnan, P., 1998: Determination of the Atmospheric Point Spread Function by a Parameter Search. – Astronomy & Astrophysics Supplement Series **131** (126).

Krutz, U., 2011: Analytische Betrachtung optisch abbildender Sensorsysteme im Rahmen der AsteroidFinder-Mission. – Ph.D. Dissertation, Humboldt Universität, Berlin.

Mendlovic, D., Zalevsky, Z. & Konforti, N., 1997: Computation Considerations and Fast Algorithms for Calculating the Diffraction Integral. – Journal of Modern Optics **44:** 407–414.

Oertel, D., Kaiser, G., Jahn, H. & Schuster, R., 1985: CCD-Sensoren in optischen Meßanordnungen. – Radio Fernsehen Elektron **34:** 490–492.

Sandau, R. & Eckardt, A. 1996: The Stereo Camera Family WAOSS/WAAC for Spaceborne/Airborne Applications. – ISPRS XXXI Part B1 Commission **I:** 170–175.

Sandau, R., Braunecker, B., Driescher, H., Eckardt, A., Hilbert, S., Hutton, J., Kirchhofer, W., Lithopoulos, E., Reulke, R. & Wicki, S., 2000: Design Principles of the LH Systems ADS40 Airborne Digital Sensor. – IAPRS XXXIII, B1, Comm. **I:** 258–265.

Skrbek, W. & Lorenz, E., 1998: HSRS – An Infrared Sensor for Hot-Spot-Detection. – Infrared Spaceborn Remote Sensing VI, Proceedings of SPIE **3437:** 167–176.

Talbiersky, U., 2010: A new Method to Validate the Usage of Fresnel Approximation Instead of Kirchhoff Diffraction Formula for Calculations Concerning Camera Systems. – Proceedings of SPIE **7717**.

Addresses of the Authors:

Ulrike Krutz, Anko Börner, Herbert Jahn, Carsten Paproth, Patrick Scherbaum and Emanuel Schlüssler, DLR German Aerospace Center, Department of Optical Information Systems at the Institute of Robotics and Mechatronics, Rutherfordstr. 2, 12489 Berlin, Germany, Tel.: +49-30-67055-511, -509, -510, -566, -502, -571, Fax: +49-30-67055-385, e-mail: first name.last name@dlr.de (ö = oe, ü = ue)

Manuskript eingereicht: September 2011
Angenommen: November 2011